RSC Advances

ROYAL SOCIETY OF CHEMISTRY

www.rsc.org/advances

In-situ preparation and characterization of conductive and magnetic nanocomposite of polypyrrole and copper hydroxychloride

Subramanyam Kasisomayajula, Niteen Jadhav and

Victoria Johnston Gelling

Abstract

Nanocomposite of conductive polypyrrole and ferrimagnetic copper hydroxychloride ($Cu_2Cl(OH)_3$) was prepared in single step via in-situ chemical oxidation of pyrrole using $CuCl_2$ as an oxidizing agent. In this work, it was shown that by monitoring the reaction time and conditions, the physical and chemical properties of polypyrrole and $Cu_2Cl(OH)_3$ in the nanocomposite can be easily controlled. This resulted in the nanocomposite with optimized conductivity and magnetic properties for wide variety of applications such as magnetic recording, electromagnetic shielding, sensors, and spintronic devices. Conductivity (0.0006S/cm – 33S/cm) and magnetization (10.25emu/mol – 53.39 emu/mol) of the nanocomposite within the range suitable for these applications were obtained by controlling the reaction conditions and thus the composition of nanocomposite. With FTIR, XPS and UV-vis spectroscopy, it was observed that as the reaction proceeds with time under controlled conditions, the oxidation of pyrrole in the presence of $CuCl_2$ leads to significant structural changes in polypyrrole as well as a gradual precipitation of $Cu_2Cl(OH)_3$. XRD and SEM analysis showed the effect of reaction conditions on the crystallinity and the morphology of polypyrrole/$Cu_2Cl(OH)_3$ nanocomposite. While the chemical and structural variations in polypyrrole were correlated with the conductivity of nanocomposite measured via Conductive-AFM technique, the changes in magnetic properties of nanocomposite were mainly attributed to the variations observed in the crystallinity of $Cu_2Cl(OH)_3$.

Keywords: Polypyrrole, $Cu_2Cl(OH)_3$, conducting and magnetic nanocomposite materials

[a] *Corresponding author. Tel.: +1 701.306.5156*
[b] *Email: kasi@autonomicmaterials.com*
[c] *Department of Coatings and Polymeric Materials, North Dakota State University, Fargo, ND 58102, USA.*

1. Introduction

Conducting polymer nanocomposites containing magnetic inorganic materials have recently attracted much attention due to their combined electrical, optical and magnetic properties.[1-3] They offer potential applications for spintronics, memory devices, sensors, microwave absorption devices, and electromagnetic shielding.[4-8] Among these conducting polymer nanocomposites, polypyrrole nanocomposites with various magnetic inorganic materials have been found to have better prospects for afore-mentioned applications because of the good environmental stability, adequate conductivity and excellent redox properties of polypyrrole.[9, 10] Several successful attempts have been made in synthesizing these composites with the combination of enhanced magnetic and conducting properties.[11-14] Most of these reports have demonstrated the synthesis and properties of these composites where magnetic inorganic particles such as Fe_xO_y, Fe_2O_3, γ-Fe_2O_3 and SiO_2 were coated with conducting polymers via chemical or electrochemical oxidation methods. The presence of nanoparticles of these magnetic inorganic materials in the composite was demonstrated by characterizing new peaks of magnetic material in FTIR.[15, 16] For example, the interaction between polypyrrole and Fe_2O_3 nanoparticles was investigated by studying chemical structure of polypyrrole in FTIR and the microstructural differences between polypyrrole/Fe_2O_3 nanocomposite in SEM. In contrast to commonly observed network structure of pure polypyrrole, the microstructures of nanocomposite with different loadings of Fe_2O_3 exhibited distinctly separated nanoparticles of polypyrrole/Fe_2O_3.[15] However, some of the inorganic materials such as Fe_3O_4 are very susceptible to oxidation owing to their high chemical activity.[17] Moreover, during functionalization of nanoparticles with conducting polymers, these nanoparticles without any surface modifications are susceptible to aggregation due to their large surface area to volume ratio resulting in poor dispersibility.[18]

Another challenge in preparation of conductive and magnetic nanocomposite via incorporation of magnetic nanoparticles into conductive polymer matrix by either chemical oxidation or electrochemical methods is the dissolution of magnetic nanoparticles in the acidic solution.[15] In the work of Guo et al., longer reactions caused the particle loss due to dissolution during the nanocomposite preparation. As a result, the nanocomposite prepared via this method did not exhibit any magnetic hysteresis. In addition, the dissolution of magnetic nanoparticles also caused inhibition to the polymerization of pyrrole leading to lower yields of polypyrrole.[15]

Enhancement of magnetic properties of composites can be attributed to not only a proper dispersion of the magnetic nanoparticles but also to their crystallinity and morphology.[19] Sunderland et

al. demonstrated that the magnetic properties of nanocomposite closely associate to the crystallinity of inorganic component in the nanocomposite.[20] γ-Fe_2O_3 nanoparticles synthesized via emulsion method at room temperature and higher temperatures were used to prepare γ-Fe_2O_3/polypyrrole nanocomposites. Higher temperatures produced nanoparticles with higher crystallinity. Nanocomposite containing these nanoparticles exhibited a significant improvement in magnetization while retaining its conductivity.[20]

The crystalline and magnetic properties of $Cu_2Cl(OH)_3$ (atacamite or clinoatacamite), a naturally occurring copper mineral, has been widely studied because of its ferrimagnetic behavior. This mineral is found to exhibit the highest coercive field in copper compounds.[21, 22] As per our knowledge, there is no report on in-situ synthesis of polypyrrole/$Cu_2Cl(OH)_3$ nanocomposite via mechanistic study. In our present work, we have attempted to synthesize polypyrrole/$Cu_2Cl(OH)_3$ nanocomposite in single step via oxidative reaction of pyrrole in the presence of $CuCl_2$ under controlled conditions. The mechanistic study on the reaction provided the information including the formation rates of polypyrrole and $Cu_2Cl(OH)_3$ as well as the required conditions to control the formation rates. In addition, conductivity measurements showed that the conductive properties of the resultant nanocomposite predominantly depend on the quality and quantity of polypyrrole incorporated into the nanocomposite. Similarly, the magnetization tests confirmed that the magnetic properties of the resultant nanocomposite mainly rely on the characteristics of $Cu_2Cl(OH)_3$ deposited in the nanocomposite. The characteristics of both polypyrrole and $Cu_2Cl(OH)_3$ in the nanocomposite were analyzed using various techniques such as Fourier transform infrared (FTIR) spectroscopy, X-ray photoelectron spectroscopy (XPS), powder X-ray diffraction (XRD), Elemental analysis (EA), and scanning electron microscopy (SEM) in order to understand the effect of morphological and structural properties of both polypyrrole and $Cu_2Cl(OH)_3$ on the conductive and magnetic properties of the resultant nanocomposite.

2. Experimental

2.1. Synthesis of polypyrrole/$Cu_2Cl(OH)_3$ nanocomposite

Pyrrole purchased from Sigma Aldrich was vacuum distilled and stored in refrigerator near around 0°C prior to use. $CuCl_2$ was also purchased from Sigma Aldrich. For synthesis, aqueous solutions of pyrrole and $CuCl_2$ of equal molar ratios (1:1) were slowly and simultaneously added, while stirring, into a closed round bottom flask at room temperature. Six different reactions were performed by varying the reaction time from t=1h to t=6h. Depending on the polymerization rate of pyrrole and formation rate of $Cu_2Cl(OH)_3$, the product of each reaction may contain varying percentages of polypyrrole and $Cu_2Cl(OH)_3$. Therefore, to analyze the composition as well as the properties, the final

products of these reactions were collected from precipitate after completion of each reaction time, washed with Millipore water, dried in oven at 60°C for 1h, and labelled as R1, R2, R3, R4, R5 and R6 respectively.

2.2. Characterization

2.2.1. Kinetic study of reaction using UV-Vis spectrophotometer

The kinetics of polymerization of pyrrole and formation of $Cu_2Cl(OH)_3$ can be obtained by observing the disappearance of pyrrole and Cu^{2+} in the reaction solution. UV-Vis-NIR Varian Cary 5000 spectrophotometer was used to find out the concentrations of pyrrole, Cu^{2+} and Cu^{+} in the reaction solutions of the above-mentioned six reactions.

An aliquot from each reaction solution was taken; and pyrrole, oligomers, Cu^{2+} and Cu^{+} were separated using hexane/water mixture into two separate solutions of hexane containing pyrrole and oligomers, and water containing $Cu^{2+}$and Cu^{+}. For measurement of pyrrole concentration, the maximum absorption of pyrrole, which occurs between 210-220nm was observed. In the case of measurement of Cu^{+} and Cu^{2+}, Bicinchoninc acid (BCA) method, which is normally used for protein analysis was used to make complex specifically with Cu^{+}. Using this method, the maximum absorption of Cu^{+}-BCA complex, which gives strong purple color at 560nm was measured to obtain the concentrations of both Cu^{+} and Cu^{2+}.

2.2.2. Characterization of polypyrrole/$Cu_2Cl(OH)_3$ nanocomposite

Prior to the characterization, all samples were grounded into fine powders. For Fourier transform infrared (FTIR) spectroscopy, the samples were prepared by making pellets using 95% of KBr and 5% of the respective nanocomposite sample. Nicolet FTIR spectrometer was used for the FTIR characterization. A JEOL JSM-6300 scanning electron microscope was used to obtain the micrographs for morphology of samples. The samples for SEM were prepared by sprinkling the ground powder onto carbon tape, which was attached to aluminum mounts. The magnification (X15,000), accelerating voltage (15 kV), and the scale (1 μm) were specified on each micrograph. For elemental analysis, the LECO CHNS-932 elemental analyzer was used to determine the amounts of carbon, hydrogen, and nitrogen, present in a sample of approximately 1 mg. The XPS measurements were performed on an SSX-100 system (Surface Science Instruments), equipped with a monochromated Al K_α X-ray source, a hemi-spherical sector analyzer (HSA) and a resistive anode detector. The samples were mounted on a sample stage using adhesive Al tapes on top of double-side carbon tapes. The base pressure of the XPS

system was 2.0 X 10^{-10} Torr. During the data collection, the pressure was 4.0 X 10^{-9} Torr. The X-ray spot size was 1 X 1 mm^2, which corresponded to an X-ray power of 200 W. The survey spectra were obtained with 15–25 scans at 150 eV using 1 eV/step. Powder X-ray diffraction (XRD) data were collected in Bragg-Brentano geometry using a Rigaku Ultima IV multipurpose XRD instrument of Rigaku. A Cu Kα X-ray radiation was used running at 40 kV with current at 44 mA. Phase identification was achieved with the help of software, JADE 9.0.

Veeco Dimension 3100 atomic force microscope with contact mode and current sensing probe was used as C-AFM to characterize the coatings prepared on aluminum substrate for surface morphology and current density. The platinum-iridium (Pt/Ir) coated cantilevers (Model: SCM-PIC, 0.01-0.025 ohm-cm Antimony (n) doped Si, spring constant 0.25 N/m) were purchased from Veeco Instruments. The bias voltage between the substrate and the coatings was varied from 100mV to 3V depending on the conductivity of sample.

Thermo-magnetic studies were completed with a Quantum Design (QD) Physical Properties Measurement System (PPMS) using the ACMS options for measurement of the magnetization as a function of applied field and temperature. Samples were put into pharmaceutical gel cup mounted into a diamagnetic plastic straw.

3. Results and discussion

Initially the samples R1 to R6 were analyzed using chemical characterization such as XRD, FTIR, XPS and elemental analysis. The changes in the chemical structure of polypyrrole and the presence of $Cu_2Cl(OH)_3$ and its degree of crystallinity were studied with respect to the reaction time. Later SEM analysis was used to correlate the structural changes in polypyrrole and $Cu_2Cl(OH)_3$ with the morphology of the resultant nanocomposite. The reaction kinetics investigated using UV-Vis spectroscopy facilitated to determine the formation rates of polypyrrole and $Cu_2Cl(OH)_3$. Finally, as illustrated by C-AFM and magnetization results, the structural and morphological properties of individual components reflected in optimized conductive and magnetic properties of the final nanocomposite.

3.1. XRD analysis

Figure 1 shows the XRD patterns of R1 to R6. The crystalline peaks in R2 to R6 correspond to atacamite and clinoatacamite, which are two types of crystalline forms of $Cu_2Cl(OH)_3$ as found from

power diffraction file (PDF) data. XRD pattern of R1 shows no crystalline peaks indicating the absence of $Cu_2Cl(OH)_3$.

The amorphous region in between two-theta of 10 and 30 in XRD spectrum of R1 represents the polypyrrole.[23] From the XRD patterns of R2 to R3, it was noticed that the intensity of crystalline peaks increased and the area of amorphous region reduced. It indicates that the formation rate of $Cu_2Cl(OH)_3$ was higher in between t=2h and t=3h of reaction time. From R3 to R6, the intensity of crystalline peak of $Cu_2Cl(OH)_3$ were reduced with the formation of new amorphous region in between two-theta of 40 and 50. The reduction of crystalline region of $Cu_2Cl(OH)_3$ that occurred significantly from R4 to R6 was a clear indication that the longer reaction times would affect the crystalline nature of $Cu_2Cl(OH)_3$. The dominating amorphous nature of nanocomposite in the samples R5 and R6 can be attributed to the formation of amorphous $Cu_2Cl(OH)_3$ causing the reduction in intensity of crystalline peaks. Thus, the reaction process appears to undergo probably in three major steps: (i) oxidation of pyrrole by $CuCl_2$ leads to the formation of polypyrrole, which continuously takes place during the entire reaction, (ii) formation of crystalline $Cu_2Cl(OH)_3$, and (iii) formation of amorphous $Cu_2Cl(OH)_3$. The reaction mechanism and formation rates of polypyrrole and $Cu_2Cl(OH)_3$ were discussed in detail in the later sections of this paper.

3.2. FTIR analysis

The broad band in R1 at 3426 cm^{-1} shown in Figure 2 could be attributed to N-H stretching vibrations of polypyrrole.[24] This peak was slightly split into two peaks in R2 and gradually developed into sharp peaks in R3 to R6. However, hydroxyl groups of atacamite ($Cu_2Cl(OH)_3$) that happen to appear anywhere in between 3450 cm^{-1} to 3330 cm^{-1} in the FTIR spectrum of atacamite were overlapped with the N-H stretching vibrations of polypyrrole.[25]

In the spectra of all samples, the characteristic peaks of polypyrrole below 1700cm^{-1} were identified.[26] The band at 1478cm^{-1}, which corresponds to C-N stretching vibration in pyrrole ring, was found to exhibit substantial changes with the reaction time. This band gradually disappeared from R1 to R6 and a new band formation at 1404cm^{-1} occurred in R5 and R6. The reduction in the intensity of C-N stretch at 1478cm^{-1} relative to the intensity of C=C stretch at 1551 cm^{-1} indicates over-oxidation of polypyrrole and loss of conjugation.[27] Changes in the shape and slight shifts in the band frequencies of C-H or C-N in-plane deformation at 1309cm^{-1}, the breathing vibration of the pyrrole ring at 1184cm^{-1}, and the C-H or N-H in-plane deformation bands at 1046cm^{-1} also occurred with time indicating probable

changes in the backbone of polypyrrole. The mode of in-plane deformation vibration of N^+H_2, which is generally located at 1093cm^{-1}, is an indication of protonation of pyrrole rings and oxidized state of polypyrrole.[28] This peak was clearly visible in R1 and R2. However, the broadening of the peaks at 1184 cm^{-1} and 1046cm^{-1} in R3, R4, R5, and R6 indicates the formation of unsymmetrical backbone of polypyrrole due to over-oxidation. As the deprotonation occurs as a result of over-oxidation, the conversion of C-N and N^+H_2 groups into C-OH and NH_4^+ that can be located around 1404cm^{-1} in the spectra of R5 and R6 takes place. The strong bands below 1000cm^{-1} in R1 are characteristic peaks of doped polypyrrole.[29] While polypyrrole continued to remain in doped state in R2 to R6 with subtle changes in these bands, new bands were formed in these region that might mainly correspond to the ($Cu_2Cl(OH)_3$).

3.3. Elemental composition analysis

As shown in Table 1, the ratio C/N was estimated to be approximately 4 for all the samples. The ratio of H/N in R1 and R2 was close to 3.14, which is normally observed in linear or branched polypyrrole.[30] From R3 to R6, it gradually increased from 3.16 to 5.10. This increase can occur due to over-oxidation or loss of conjugation in polypyrrole as well as due to the formation of $Cu_2Cl(OH)_3$.

Table 1: Elemental composition and %yields of samples from R1 to R6

Label	N (Mass%)	C (Mass%)	H (Mass%)	Empirical Formula for polypyrrole	Cu (Mass%)	Yield of composite (%)
R1	15.84	54.11	3.57	$C_{3.99}H_{3.16}N$	0.444	3-5%
R2	13.21	42.94	2.96	$C_{3.79}H_{3.14}N$	1.19	10-12%
R3	9.85	33.17	2.35	$C_{3.92}H_{3.34}N$	2.413	23-25%
R4	10.48	35.24	3.28	$C_{3.92}H_{4.38}N$	2.502	35-40%
R5	11.04	37.76	3.94	$C_{3.99}H_{4.99}N$	3.254	42-45%
R6	11.11	37.99	4.05	$C_{3.99}H_{5.10}N$	4.009	48-55%

3.4. XPS analysis

The increase in N-H at 400eV from t=3h (R3) to t=4h (R4) in Figure 3 reflected in decrease of C=N and C-N^+. This can be attributed to the loss of charge on pyrrole rings or loss of conjugation due to over-oxidation.[31] While N-H percentage remained constant in 1h, 2h, and 3h samples, some of the C=N groups apparently converted to C-N^+ from sample 1 to 3 probably due to the protonation and subsequent incorporation of dopant ion. From 3h onwards, both C=N and C-N^+ groups started converting into N-H groups with apparent loss of conjugation.

Figure 4 shows the curve fitting of high resolution XP spectra of copper present in samples R1 to R6. The peak fitting shows four peaks of which two peaks for core Cu $2p_{3/2}$ level consisting of two binding energy states at 932.4eV and 934.6eV, and other two peaks for its corresponding shake-up satellites at 941.4eV and 944.5eV. As shown in Figure 5, the peak at 932.4eV belongs to Cu(I) and the peaks including 934.6eV, 941.4eV and 944.5eV belong to Cu(II).[32] Interestingly, the peak intensity at 932.4eV corresponding to Cu(I) was found to vary substantially from R2 to R3 and then from R5 to R6. These changes occurred most likely due to the variations in the conversion rate of CuCl to $Cu_2Cl(OH)_3$ as directed by the reaction conditions. The effect of the reaction conditions on the conversion rate was explained in detail in the next section.

3.5. Kinetics of reaction using UV-Vis spectrophotometer

Standard curves for pyrrole and Cu(I) shown in Figure 5(a) and 5(b) were obtained from their corresponding stock solutions. Different concentrations of solutions of pyrrole in hexane were used to obtain the relationship between concentration and absorbance. It was found in our experiments that the maximum absorption of pyrrole between 210-220nm for concentrations between 1mM to ~8mM follows a logarithmic or exponential growth relationship between the absorbance and the concentration (Figure 5(a)). A standard procedure was followed in order to obtain standard curve for Cu(I).[33] Different concentrations of Cu(II) solutions in Millipore water were made using $CuCl_2$ and used to prepare equivalent concentrations of Cu(I) solutions by adding hydroxylamine to each of them. As shown in Figure 6, the Cu(I) in solution forms complex with BCA and gives purple color with the corresponding absorbance value related to its concentration (Figure 5(b).

Figures 5(c) and 5(d) show the trends of concentrations of pyrrole, Cu(I), Cu(II) with time in the reaction mixture. The decay of pyrrole and Cu(II) concentrations were found to have linear relationship with time. The concentration of Cu(I) at anytime was very small as compared to the total concentration

of Cu(I) and Cu(II). Therefore, the trend of Cu(II) was approximately the same as for total concentration of Cu(I) and Cu(II) in solution. The trend of concentration of Cu(I) occurred due to the difference between the reduction rate of Cu(II) to Cu(I) and the conversion rate of Cu(I) to $Cu_2Cl(OH)_3$. Up on comparison between 5(c) and 5(d), it was found in this work that the disappearance of pyrrole was twice as fast as the reduction of Cu(II) to Cu(I).

Figure 7 shows the equations of reactions involved in the formation of polypyrrole and $Cu_2Cl(OH)_3$. Redox reaction between pyrrole and $CuCl_2$ oxidizes pyrrole to become pyrrole cation radical and reduces Cu(II) to Cu(I). This Cu(I) combines with chloride ion to form insoluble cuprous chloride (CuCl). As CuCl is not stable in the presence of oxygen and water, it gets oxidized, changes into stable form of Cu(II) and subsequently produces $Cu_2Cl(OH)_3$ depending on the availability of dissolved oxygen in water.[34]

3.6. SEM analysis

As shown in Figure 8, spherical particles of composite were observed in R1, R2 and R3 with particles size reduced from R1 to R2, and then increased from R2 to R3. The spherical particle shape gradually disappeared in between R3 and R4, and irregular and rectangular shape appeared in R4. This irregular shape was prominent in R5 and R6. Significant change in particle shape of composite occurred in between t=3h and t=4h. As seen previously in XRD results, the amorphous nature of $Cu_2Cl(OH)_3$ was predominant in R5 and R6. The chemical structural changes in polypyrrole and $Cu_2Cl(OH)_3$ clearly reflected in the morphological transformation from regular spherical and rectangular to irregular and clumped particles.

3.7. Conductivity Measurements

According to the literature, polypyrrole based magnetic nanocomposites can exhibit distinct conductivities depending on the kind and amount of magnetic nanoparticles incorporated into the polypyrrole matrix. Polypyrrole nanocomposites containing lower amounts (~ 1 w/v%) of Fe_2O_3, ZrO_2, and SiO_2 nanoparticles showed conductivities of 90 S/cm, 17 S/cm, and 3 S/cm respectively. Higher loadings of nanoparticles (~90 wt%) caused reduction in conductivities of nanocomposite to approximately 10^{-3} S/cm.[35] Therefore, depending on the kind of desired application, the required conductivity is normally obtained by adjusting the quantity of polypyrrole in the nanocomposite.

In our present work, all samples (R1 to R6) showed a range of conductivity values in both C-AFM and four point probe methods with the highest conductivity in the range of 25-33 S/cm displayed by R1 and lowest in the range of 0.0013 S/cm to 0.0006 S/cm displayed by R5 and R6. While I-V curves were used in C-AFM to calculate the conductivities, the voltage measured from applied current ($4.5x10^{-6}$A) was used in four-point probe method. The samples especially R1, R2, R3, and R4 showed optimum values of conductivity in the range normally desired for good EMI and microwave shielding applications.[36, 37]

Figure 9 shows the AFM-current images obtained for all samples at the same scan rate of 0.5Hz using low current sensitivity. Different DC sample voltages (bias) were required to apply in order to maintain low current sensitivity for all of them for easier comparison. The DC sample voltages applied for samples R1, R2, R3, R4, R5 and R6 were 100mV, 1V, 2V, 3.5V, 3.8V, and 3.8V respectively.

As shown in Figure 9, the current density and magnitude over 10µm X 10µm area gradually decreased from R1 (124.0 nA) to R6 (1.5 nA). Furthermore, the conductive areas in samples R5 and R6 were considerably smaller. The reduction in conductivity can be associated with the changes in two factors: (i) conjugation length/over-oxidation in polypyrrole and (ii) precipitation of non-conductive $Cu_2Cl(OH)_3$. As observed in FTIR previously, the ratio between C=N stretch at 1478 cm^{-1} and C=C stretch at 1551 cm^{-1} appeared to be higher in the case of R1 indicating higher conjugation length in polypyrrole and therefore higher conductivity. This ratio gradually reduced from R1 to R6 reflecting the decrease in conductivity of polypyrrole. XPS results also indicated that the samples R5 and R6 contained over-oxidized polypyrrole leading to lower conjugation and thereby lower conductivity. In addition to lowering of conductivity in polypyrrole due to chemical structural changes, the precipitation of non-conductive $Cu_2Cl(OH)_3$, as evidenced by elemental composition analysis, would also have caused the reduction in overall conductivity of nanocomposite.

3.8. Magnetic properties of PPy/$Cu_2Cl(OH)_3$ nanocomposite

The magnetic behavior of any material is determined by obtaining its magnetization or magnetic moment in the presence of an applied magnetic field. Ferromagnets, known for many different applications such as magnetic recording devices, computer discs, transformers, and credit cards, are the materials that can retain a memory of an applied field even after it is removed. Ferrimagnets are the materials that can exhibit ferromagnetic behavior only when they are in crystalline form. This

ferromagnetic behavior, known as hysteresis, can be acquired by plotting a hysteresis loop, which is the relationship between magnetic moment (M) and applied magnetic field (H).[38]

Polypyrrole based magnetic nanocomposites containing various types of nanoparticles were widely studied in the literature in terms of coercivities and magnetizations. In Guo et al.'s work, nanocomposites of polypyrrole-Fe_2O_3 with high particle loadings of Fe_2O_3 nanoparticles at 20wt% and 50wt% exhibited high saturation magnetizations of 29.4 emu/g and 45.1 emu/g respectively. However, high particle loading caused significant reduction in conductivity of nanocomposite.[15] Polypyrrole nanocomposites prepared with manganese zinc ferrite nanoparticles were used as soft ferrimagnetic materials for Radio Frequency (RF) and Electromagentic Interference (EMI) applications. These samples showed saturation magnetization of 0.242 emu/g and coercitivity of 510 Oe at 10K. Similarly, the nanocomposites of polypyrrole-Fe_2O_3 at small quantities of polypyrrole (0.5wt% and 10wt%) showed the saturation magnetization in the range 0.0029 – 0.0055 emu/g and coercivities of 310 Oe and 380 Oe indicating an increase in the magnetic properties with the inclusion of polypyrrole despite its diamagnetic property.[35, 39]

In our current work, the magnetization measurement of the samples R1 and R2 showed that these materials possess diamagnetic properties with no hysteresis loop.[38] As evidenced by the XRD and elemental analysis, the samples R1 and R2 mainly consist of polypyrrole as major component and therefore the magnetic property is predominantly influenced by the diamagnetic behavior of polypyrrole. Therefore, the samples R3, R4, R5 and R6 that exhibited hysteresis loop were only shown in Figure 10. At low fields, a hysteretic behavior typical for magnetically ordered materials dominated in them.[38] For evaluation purposes the linear paramagnetic contribution was subtracted and the corrected M(H) for -17kOe<H<17kOe range was shown in Figure 9.

The sample R3 showed hard-ferromagnetic property with broader hysteresis loop and higher coercivity (H_c) and remanence (M_r) (shown in red in Figure 10). As observed previously in XRD analysis, the crystalline part of $Cu_2Cl(OH)_3$ relatively reached the highest in R3, and then gradually decreased from R3 to R6. Similarly, as it can be seen in Figure 10, the ferromagnetic magnetic properties reduced from R3 to R6 indicating that these properties certainly stem from the crystalline part of $Cu_2Cl(OH)_3$. The approximate values of the coercivity (H_c) or coercive field at the temperature T=2K for samples R3, R4, R5 and R6 were 4000 Oe, 2000 Oe, 400 Oe and 500 Oe respectively. The remanence (M_r) or the saturation magnetization for these samples R3, R4, R5 and R6 were correspondingly 53.39 emu/mol (0.25 emu/g), 24.56 emu/mol (0.115 emu/g), 20.92 emu/mol (0.1 emu/g) and 10.25 emu/mol (0.05

emu/g). From the above-mentioned magnetization test results, it is clear that the ferromagnetic properties such as coercivity and remanence attain optimum level in the nanocomposite when the reaction produces maximum amount of crystalline $Cu_2Cl(OH)_3$. This result suggests that longer reaction times (greater than 3h) can cause reduction in magnetic properties due to the formation of amorphous $Cu_2Cl(OH)_3$, as observed for the samples R4, R5, and R6.

4. Conclusions

Polypyrrole/$Cu_2Cl(OH)_3$ nanocomposite has been in-situ synthesized in single step via chemical oxidation of pyrrole using $CuCl_2$ as an oxidant. The kinetics of this synthesis was studied using UV-Vis spectroscopy. In this study, it was found that while the trends of pyrrole oxidation and Cu(II) reduction were linearly dependent with time, the trend of Cu(I) followed a curvilinear due to the difference between the reduction rate of Cu(II) to Cu(I) and the conversion rate of Cu(I) to $Cu_2Cl(OH)_3$. FTIR and XPS results showed the disappearance of CN bond and CN^+ due to over-oxidation of polypyrrole. Moreover, the appearance of hydroxyl groups was observed in FTIR confirming the gradual formation of $Cu_2Cl(OH)_3$. The high-resolution XP spectra of copper revealed that the conversion rate of Cu(I) to $Cu_2Cl(OH)_3$ would depend on the availability of dissolved oxygen. After t=3h of reaction time, the reduction in crystallinity was observed in XRD and the irregular morphology was seen in SEM. Over-oxidized polypyrrole and amorphous $Cu_2Cl(OH)_3$ resulted in lower conductivities and poor magnetization properties as the reaction progressed for longer times. Thus, from these studies, it can be concluded that by controlling the reaction conditions, the properties such as conductivity and magnetic properties of polypyrrole/$Cu_2Cl(OH)_3$ nanocomposite can be optimized.

Acknowledgements

The authors would like to thank the U.S. Army Research Laboratory under grant no. W911 NF-04-2-0029, W911NF-09-2-0014, W911NF-10-2-0082, and W911NF-11-2-0027 for supporting this research.

References

1. P. Gomez-Romero, *Advanced Materials*, 2001, **13**, 163-174.
2. K. Rajeshwar, N. de Tacconi and C. Chenthamarakshan, *Chem. Mater*, 2001, **13**, 2765-2782.
3. R. Gangopadhyay and A. De, *Chem. Mater*, 2000, **12**, 608-622.

4. W. Naber, S. Faez and W. Wiel, *Journal of Physics D: Applied Physics*, 2007, **40**, R205.

5. V. I. Krinichnyi, H. K. Roth and M. Schrodner, *Appl. Magn. Reson.*, 2002, **23**, 1-17.

6. T. Otero, *Bioinspiration & Biomimetics*, 2008, **3**, 035004.

7. K. Singh, A. Ohlan, A. Bakhshi and S. Dhawan, *Materials Chemistry and Physics*, 2010, **119**, 201-207.

8. R. Fox, V. Wani, K. Howard, A. Bogle and L. Kempel, *Journal of Applied Polymer Science*, 2008, **107**, 2558-2566.

9. T. Vernitskaya and O. Efimov, *Russian Chemical Reviews*, 1997, **66**, 443.

10. N. Jadhav, C. A. Vetter and V. J. Gelling, *Electrochimica Acta*, 2013, **102**, 28-43.

11. L. Cabrera, S. Gutierrez, M. P. Morales, N. Menendez and P. Herrasti, *J. Magn. Magn. Mater.*, 2009, **321**, 2115-2120.

12. Y. L. Luo, L. H. Fan, F. Xu, Y. S. Chen, C. H. Zhang and Q. B. Wei, *Materials Chemistry and Physics*, 2010, **120**, 590-597.

13. L. Fang, T. Y. Dai and Y. Lu, *Synthetic Met*, 2009, **159**, 2101-2107.

14. H. Xiao, W. Zhang, M. Wan and S. Fu, *Journal of Polymer Science, Part A: Polymer Chemistry*, 2009, **47**, 4446-4453.

15. Z. Guo, K. Shin, A. Karki, D. Young, R. Kaner and H. T. Hahn, *Journal of Nanoparticle Research*, 2009, **11**, 1441-1452.

16. X. Li, M. Wan, Y. Wei, J. Shen and Z. Chen, *The Journal of Physical Chemistry B*, 2006, **110**, 14623-14626.

17. J. Zhao, R. Luque, W. Qi, J. Lai, W. Gao, M. R. Hasan Shah Gilani and G. Xu, *Journal of Materials Chemistry A*, 2015, **3**, 519-524.

18. H. Zhang, X. Zhong, J. Xu and H. Chen, *Langmuir*, 2008, **24**, 13748-13752.

19. K. Sunderland, P. Brunetti, L. Spinu, J. Y. Fang, Z. J. Wang and W. G. Lu, *Materials Letters*, 2004, **58**, 3136-3140.

20. K. Sunderland, P. Brunetti, L. Spinu, J. Fang, Z. Wang and W. Lu, *Materials Letters*, 2004, **58**, 3136-3140.

21. S. Yang, T. Li, B. Xu and Y. Du, *Journal of Physics: Condensed Matter*, 2003, **15**, 5629.

22. X. Zheng and E. Otabe, *Solid State Commun*, 2004, **130**, 107-109.

23. P. M. Carrasco, H. J. Grande, M. Cortazar, J. M. Alberdi, J. Areizaga and J. A. Pomposo, *Synthetic Met*, 2006, **156**, 420-425.

24. T. Dai, X. Yang and Y. Lu, *Nanotechnology*, 2006, **17**, 3028.

25. R. Frost, W. Martens, J. Kloprogge and P. Williams, *Journal of Raman Spectroscopy*, 2002, **33**, 801-806.

26. M. Omastová, M. Trchová, J. Kováová and J. Stejskal, *Synthetic Met*, 2003, **138**, 447-455.

27. N. V. Blinova, J. Stejskal, M. TrchovÃ¡, J. ProkeÅ¡ and M. r. OmastovÃ¡, *European Polymer Journal*, 2007, **43**, 2331-2341.

28. S. Kasisomayajula, X. Qi, C. Vetter, K. Croes, D. Pavlacky and V. Gelling, *Journal of Coatings Technology and Research*, 2010, **7**, 145-158.

29. T.-M. Wu, H.-L. Chang and Y.-W. Lin, *Polymer International*, 2009, **58**, 1065-1070.

30. B. Saunders, R. Fleming and K. Murray, *Chemistry of Materials*, 1995, **7**, 1082-1094.

31. C. Malitesta, I. Losito, L. Sabbatini and P. Zambonin, *Journal of Electron Spectroscopy and Related Phenomena*, 1995, **76**, 629-634.

32. C. C. Chusuei, M. A. Brookshier and D. W. Goodman, *Langmuir*, 1999, **15**, 2806-2808.

33. M. Anwar, M. Iqbal, M. Qamar, M. Rehman and A. Khalid, *World Journal of Microbiology and Biotechnology*, 2000, **16**, 135-138.

34. A. Caputo, L. J. Turbini and D. D. Perovic, *J. Electron. Mater.*, 2010, **39**, 92-96.

35. R. Gangopadhyay and A. De, *Chemistry of Materials*, 2000, **12**, 608-622.

36. Ã. z. Yavuz, M. K. Ram, M. Aldissi, P. Poddar and H. Srikanth, *Synthetic Metals*, 2005, **151**, 211-217.

37. Ã. z. Yavuz, M. K. Ram, M. Aldissi, V. Erokhin, M. K. Ram and O. Yavuz, in *The New Frontiers of Organic and Composite Nanotechnology*, Elsevier, Amsterdam, 2008, pp. 435-475.

38. S. N. A, in *Magnetic Materials: Fundamentals and Applications*, Cambridge University Press, 2010, ch. 9, pp. 113-129.

39. P. Poddar, J. L. Wilson, H. Srikanth, S. A. Morrison and E. E. Carpenter, *Nanotechnology*, 2004, **15**, S570.

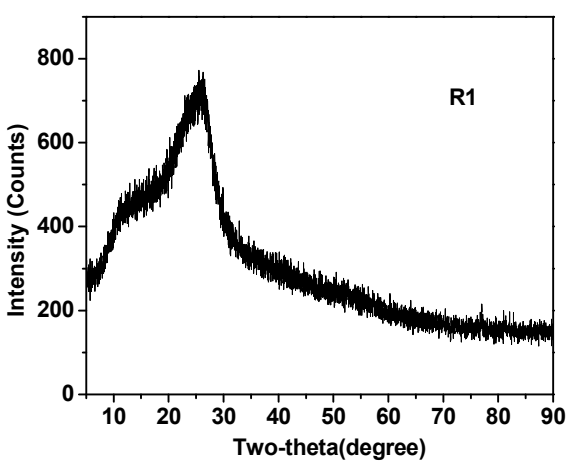

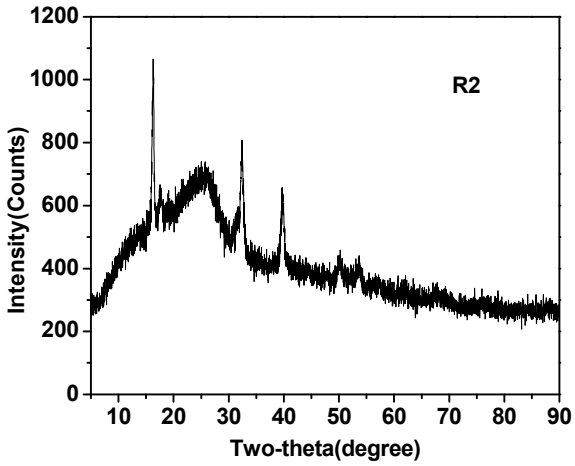

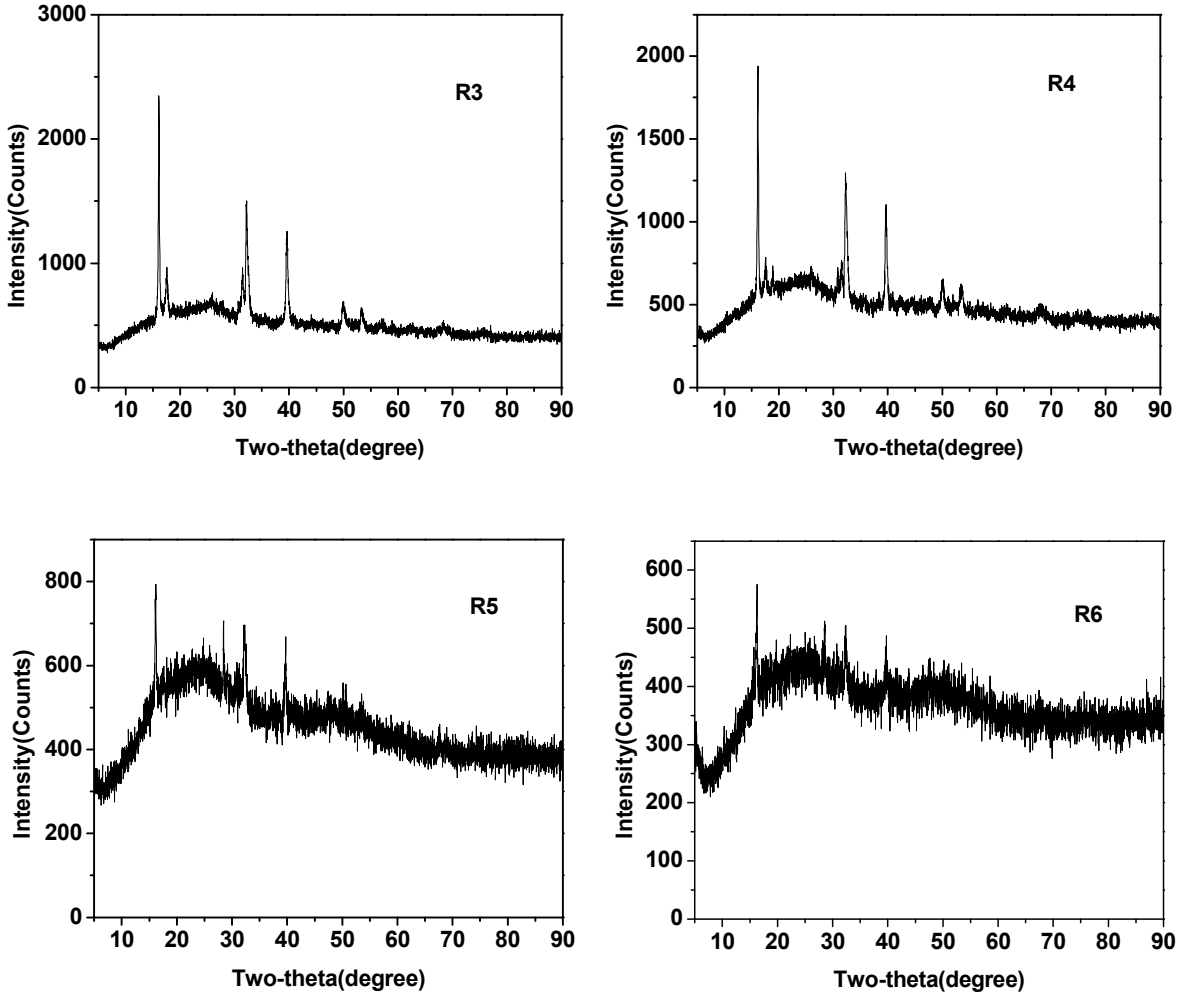

Figure 1. X-ray diffraction patterns of samples R1, R2, R3, R4, R5 and R6.

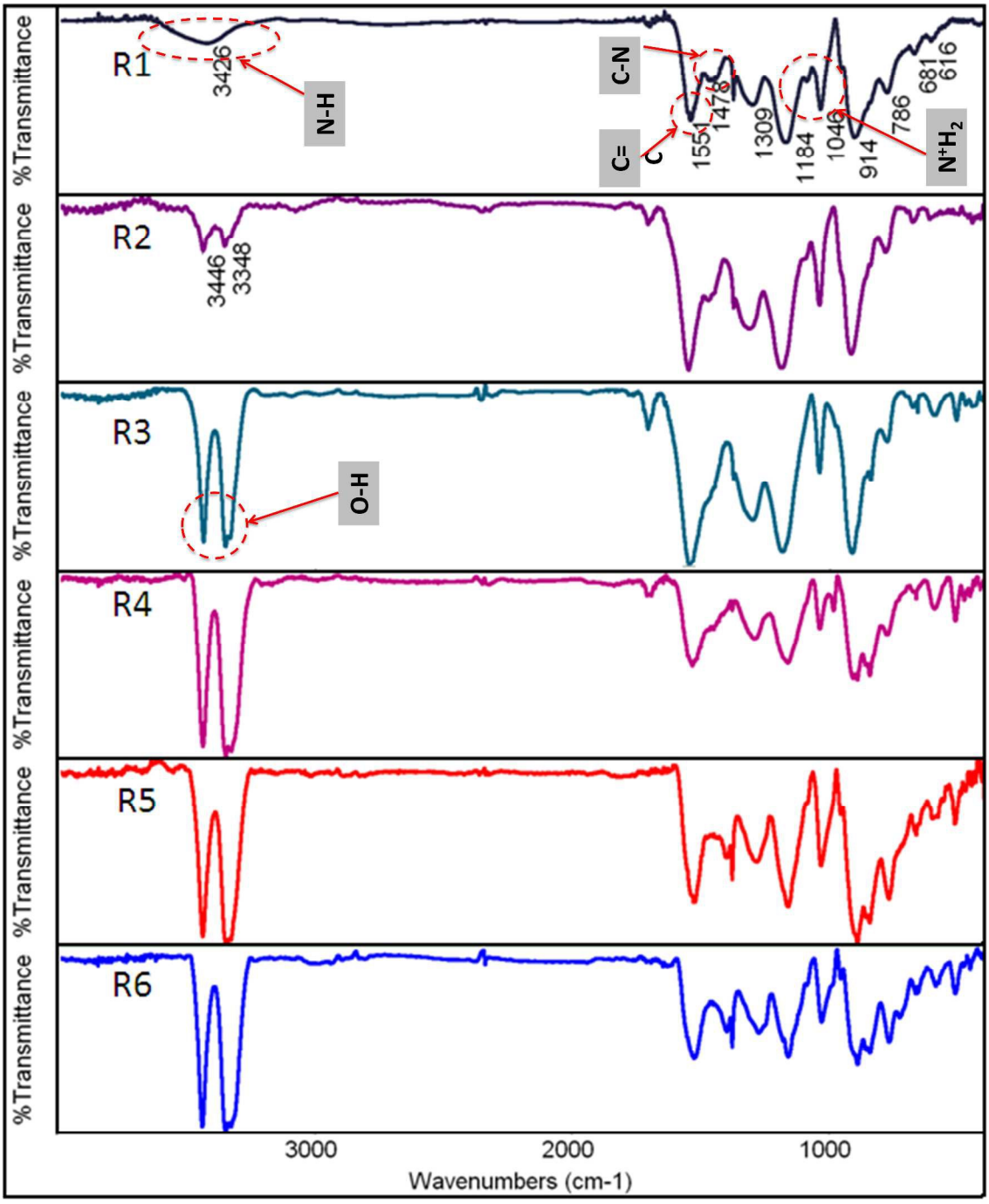

Figure 2. FTIR spectra of samples R1, R2, R3, R4, R5 and R6

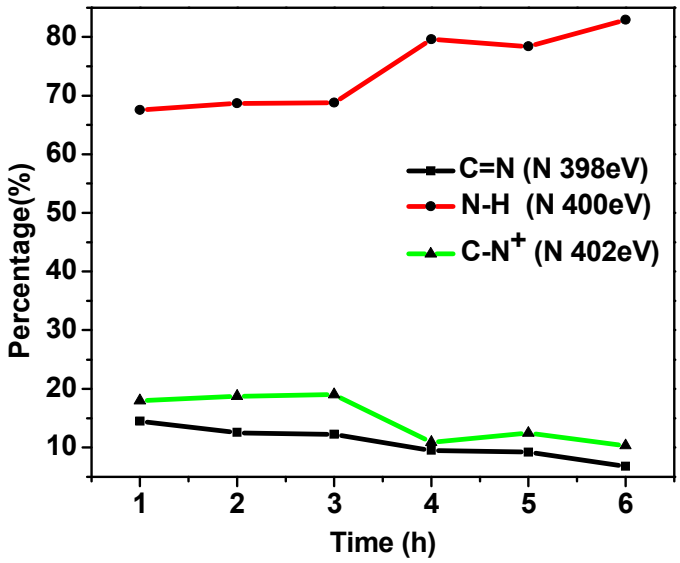

Figure 3. Percentages of chemical shifts of nitrogen in polypyrrole from high-resolution XPS analysis in samples R1 (t=1h) to R6 (t=6h)

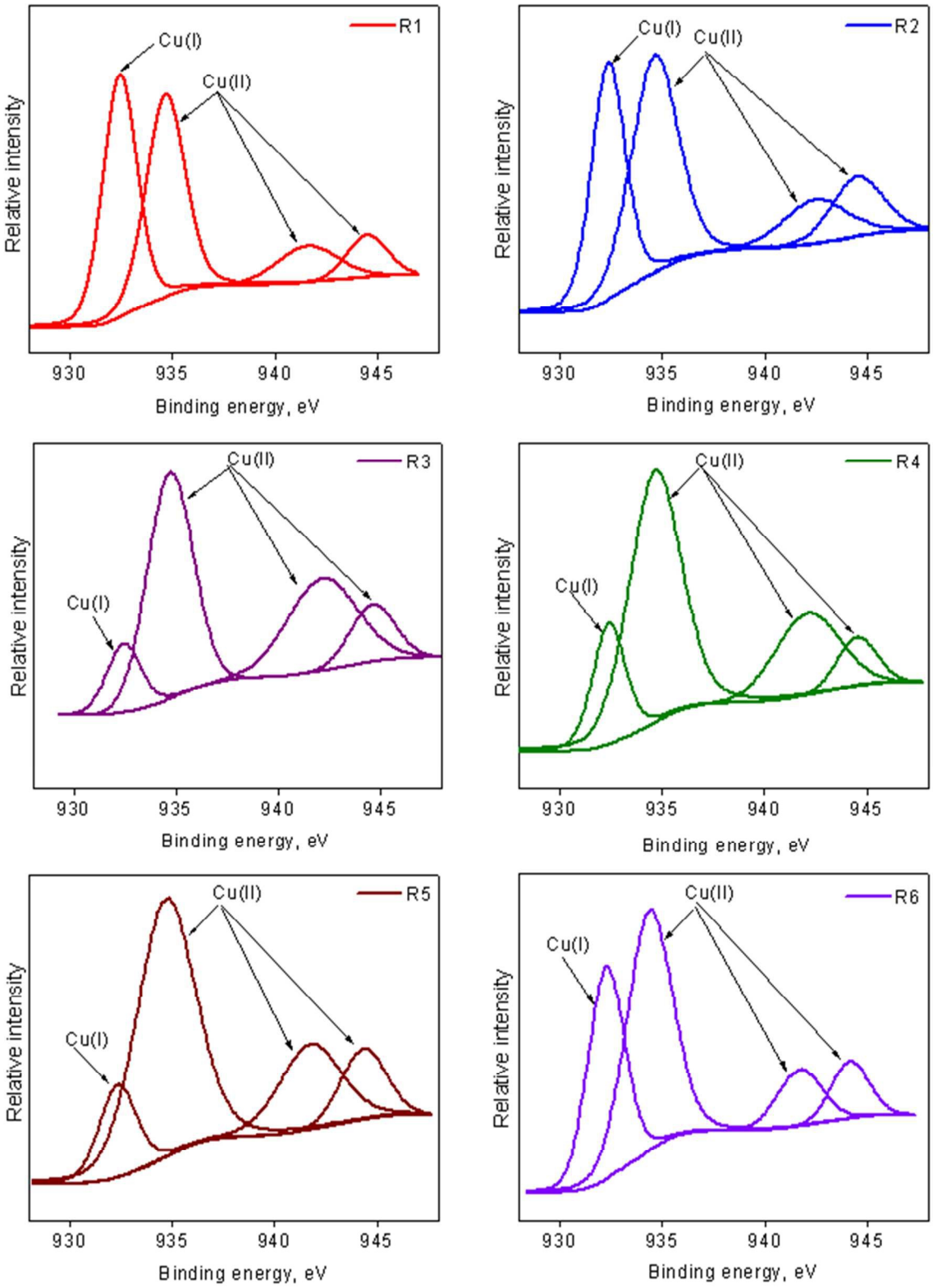

Figure 4. High-resolution XP Spectra of Copper in samples R1 to R6. The resultant components from curve fitting are shown.

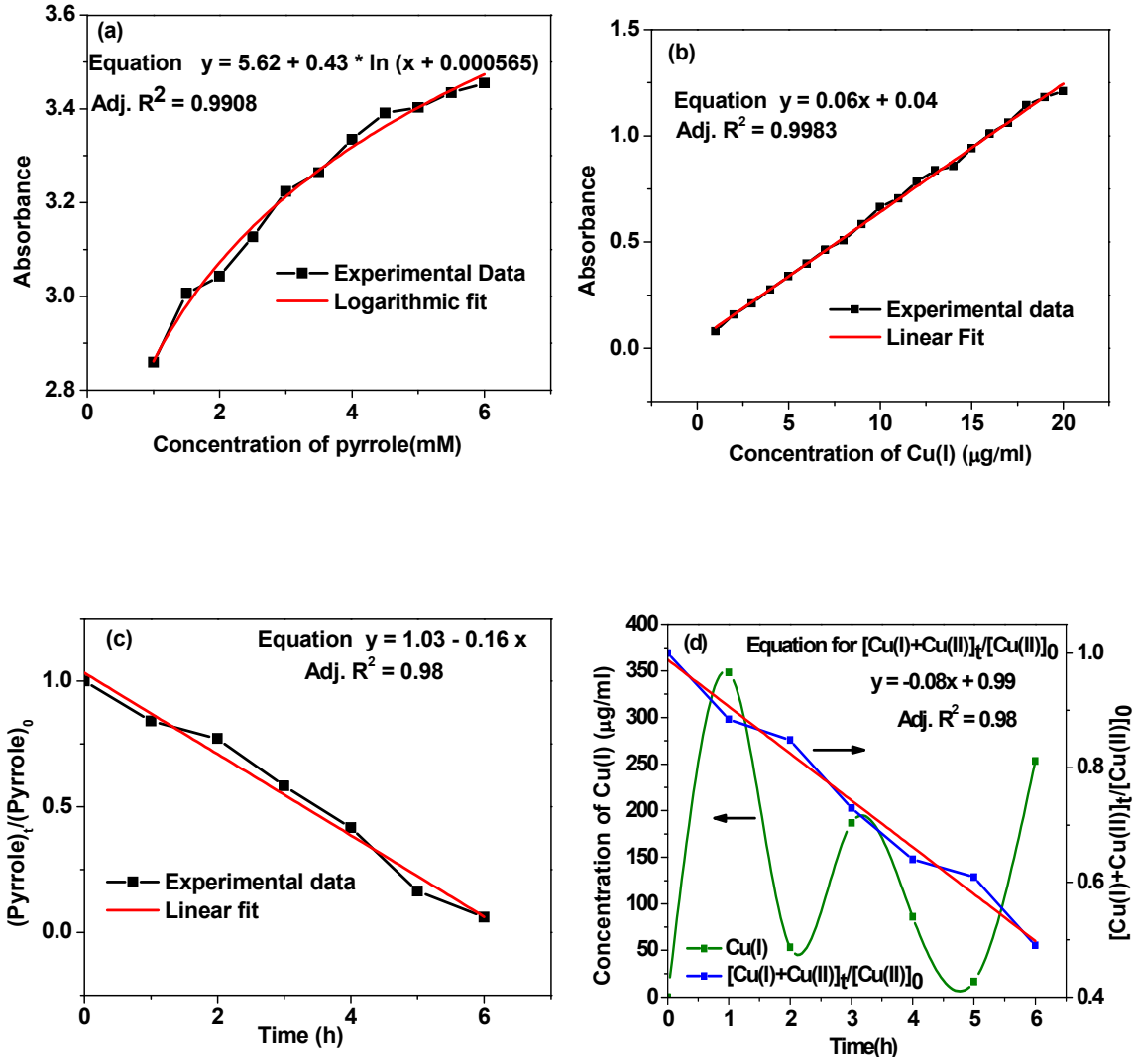

Figure 5. (a) standard curve for pyrrole, (b) standard curve for Cu(I), (c) the trend of pyrrole disappearance, (d) the trend of Cu(I), Cu(II) and the total of both Cu(I) and Cu(II)

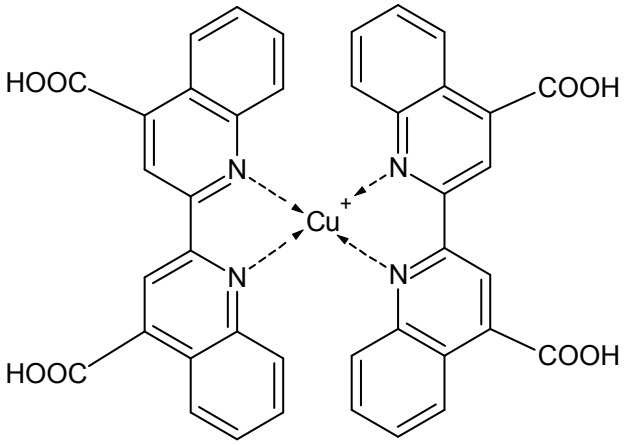

Figure 6. Purple color complex of Cu^{+}-BCA

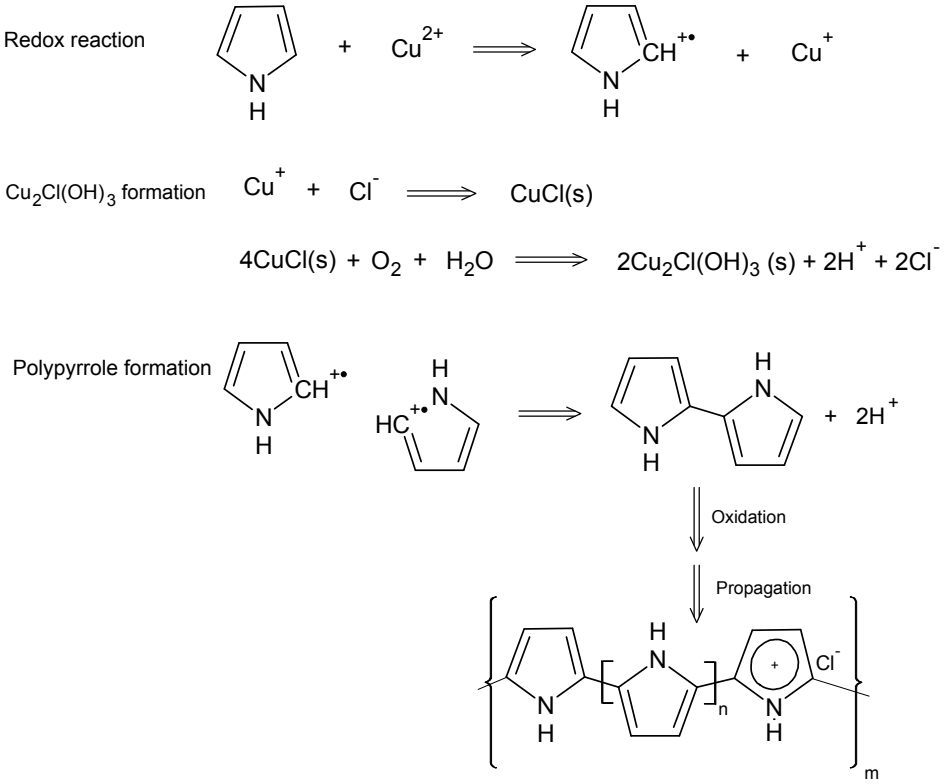

Figure 7. Reaction mechanisms of polypyrrole and $Cu_2Cl(OH)_3$ formation

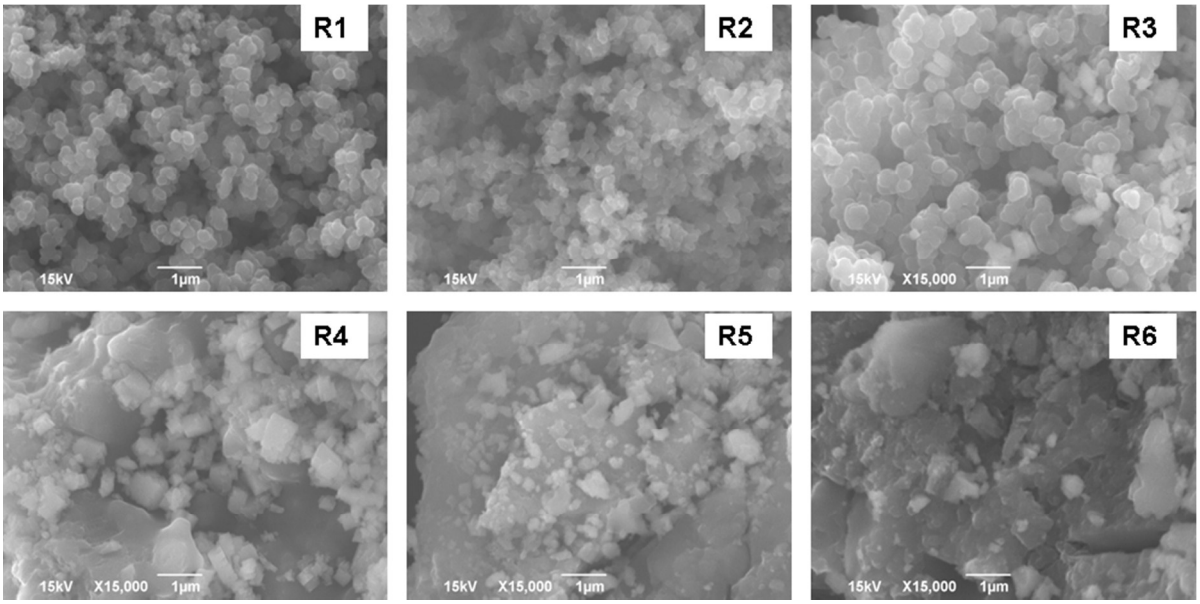

Figure 8. SEM images of samples R1, R2, R3, R4, R5 and R6

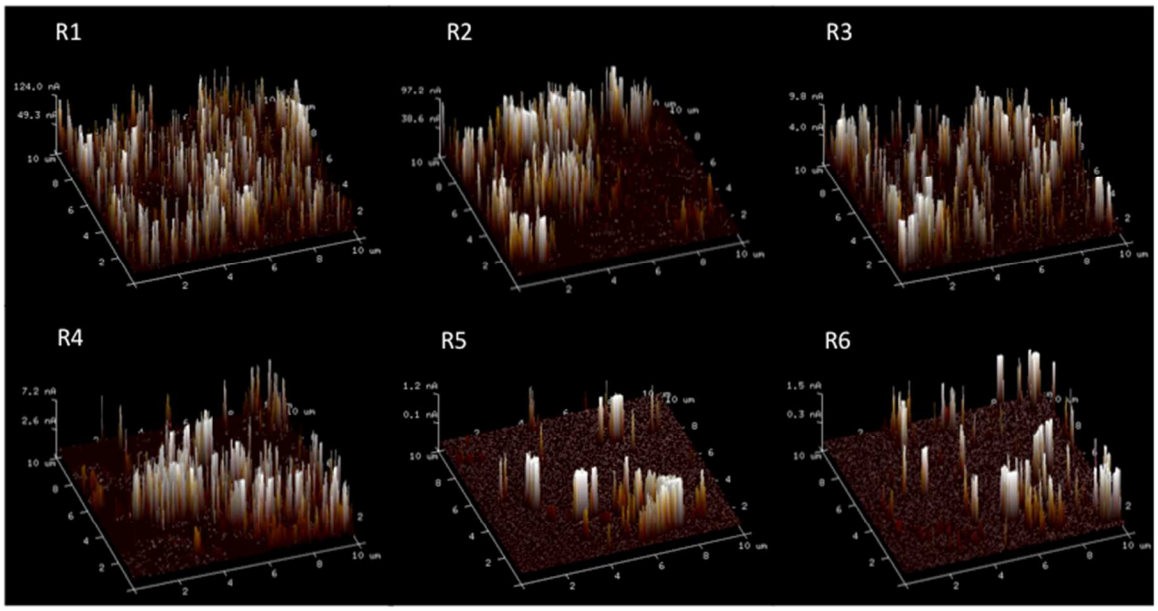

Figure 9. AFM current images of R1, R2, R3, R4, R5 and R6 (Scan rate was 0.5Hz. Low Current Sensitivity

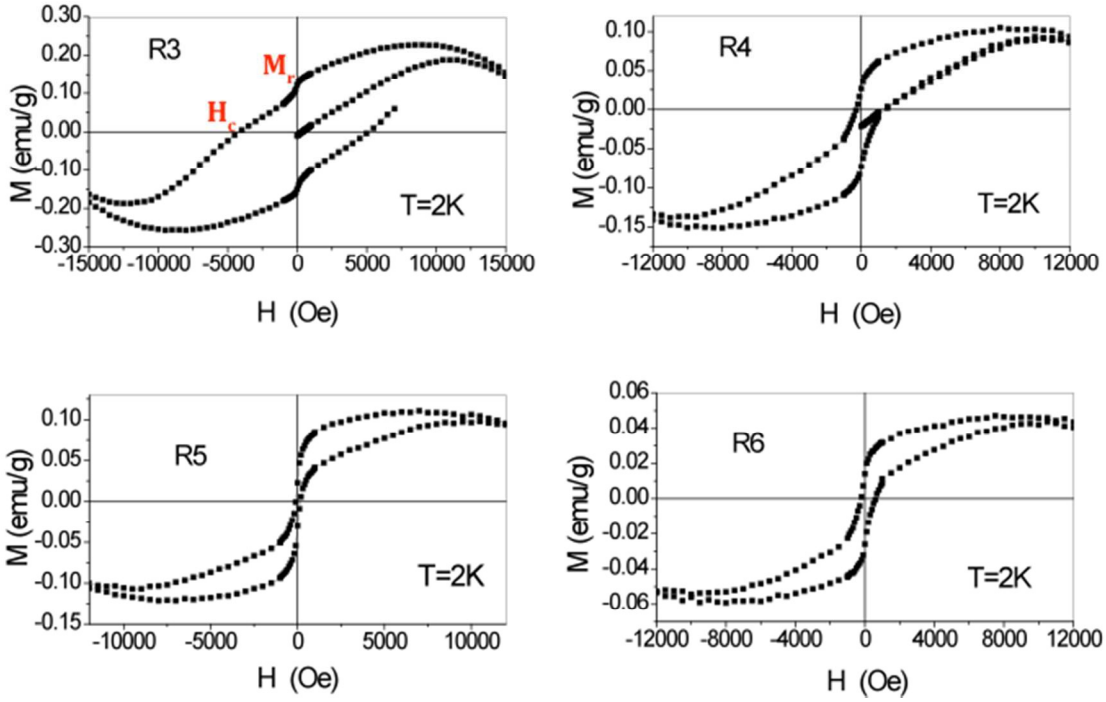

Figure 10. The magnetic hysteresis loops of samples R3, R4, R5 and R6 at T=2K after the abstraction of paramagnetic behavior

Graphical Abstract:

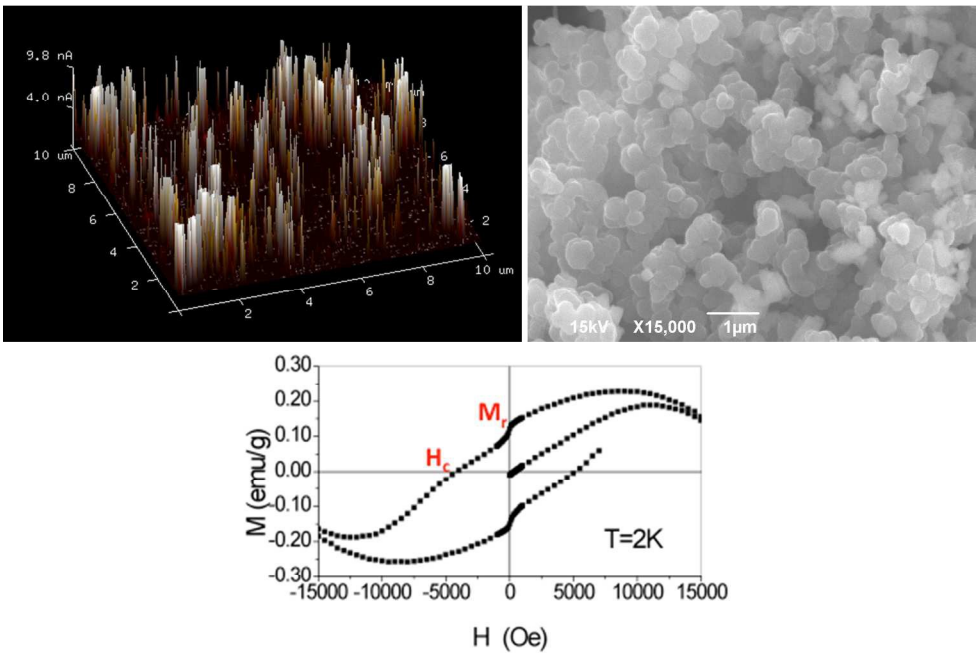

Nanocomposite of polypyrrole and copper hydroxychloride ($Cu_2Cl(OH)_3$) with combined conductive and ferrimagnetic properties was synthesized in single step in-situ chemical oxidation process.